Chinese Chemical Letters 35 (2024) 108975

Contents lists available at ScienceDirect

Chinese Chemical Letters

journal homepage: www.elsevier.com/locate/cclet

Peptidome data-driven comprehensive individualized monitoring of membranous nephropathy with machine learning

Zixing Xu[a,1], Ruiying Chen[b,1], Chuanming Hao[b], Qionghong Xie[b,*], Chunhui Deng[a,c,*], Nianrong Sun[a,*]

[a] Department of Gastroenterology and Hepatology, Zhongshan Hospital, and Department of Chemistry, Fudan University, Shanghai 200433, China
[b] Division of Nephrology, Huashan Hospital, Fudan University, Shanghai 200040, China
[c] School of Chemistry and Chemical Engineering, Nanchang University, Nanchang 330031, China

ARTICLE INFO

Article history:
Received 26 April 2023
Revised 1 August 2023
Accepted 24 August 2023
Available online 1 September 2023

Keywords:
Membranous nephropathy
Serum peptidome
Machine learning
Disease diagnosis

ABSTRACT

As the most common pathological type of nephrotic syndrome, membranous nephropathy (MN) presents diversity in progression trends, facing severe complications. The precise discrimination of MN from healthy people, other types of nephrotic syndrome or those with therapeutic remission has always been huge challenge in clinics, not to mention comprehensive individualized monitoring relied on minimally invasive molecular detection means. Herein, we construct a functionalized pore architecture to couple with machine learning to aid all-round peptidome enrichment and data profiling from hundreds of human serum samples, and finally establish a set of defined peptide panel consisting of 12 specific feature signals. In addition to the realization of above-mentioned precise discrimination with more than 97% of sensitivity, 88% of accuracy and f1 score, the simultaneously comprehensive individualized monitoring for MN can also be achieved, including conventionally screening diagnosis, congeneric distinction and prognostic evaluation. This work greatly advances the development of peptidome data-driven individualized monitoring means for complex diseases and undoubtedly inspire more devotion into molecular detection field.

Membranous nephropathy (MN), an autoimmune kidney disease caused by immune deposition along the subepithelial region of the glomerular filtration barrier [1,2], is the most common pathological type of nephrotic syndrome [3]. Without precise diagnosis and subsequently reasonable therapeutic protocols, most of MN patients will develop into chronic kidney disease suffering from long-time pain, or deteriorate into end-stage renal disease facing the threat of high-mortality, or tightly entangle with other diseases such as systemic lupus erythematosus, other autoimmune diseases, infection and cancer [4–6]. In other word, there are two main issues for now to be addressed to avoid the progression of MN towards a bad direction. For one thing, although the respective sensitivity of podocyte antigens phospholipase A2 receptor (PLA2R) and thrombospondin type 1 domain-containing protein 7A (THSD7A) are merely about 70% and 3%, their sequential combination still becomes the common strategy because of the lack of better diagnostic means [7–9], Moreover, MN has similar clinical manifestation to other subtypes of nephrotic syndrome such as minimal change disease (MCD) [10], but totally different therapeutic protocols [11], whereas their discrimination can only rely on renal biopsy with serious invasiveness and high equipment requirements [12,13]. For another, the clinics carry out prognosis evaluation based on anti-PLA2R1 antibody levels, during which the use of some toxic agents was a huge question [14–16]. Therefore, it is of utmost implications to develop an advanced means with high sensitivity and low damage to enable comprehensive individualized monitoring of MN, including precise diagnosis and prognosis monitoring.

Omics molecule-driven disease diagnosis and monitoring have always been recognized as the shining star in clinics and drew increasing attention in the past decades [17,18]. However, disease detection researches on sequencing-based genomics and transcriptomics are high-cost [19,20], LC-MS-based proteomics and metabolomics are time-consuming, both of them are not the best appropriate means to realize individualized monitoring of diseases at the age of precision medicine [21,22]. Generally speaking, the significant premise for screening specific molecular features in pre-

* Corresponding authors.
E-mail addresses: qionghongxie@fudan.edu.cn (Q. Xie), chdeng@fudan.edu.cn (C. Deng), sunnianrong@fudan.edu.cn (N. Sun).
[1] These authors contributed equally to this work.

https://doi.org/10.1016/j.cclet.2023.108975
1001-8417/

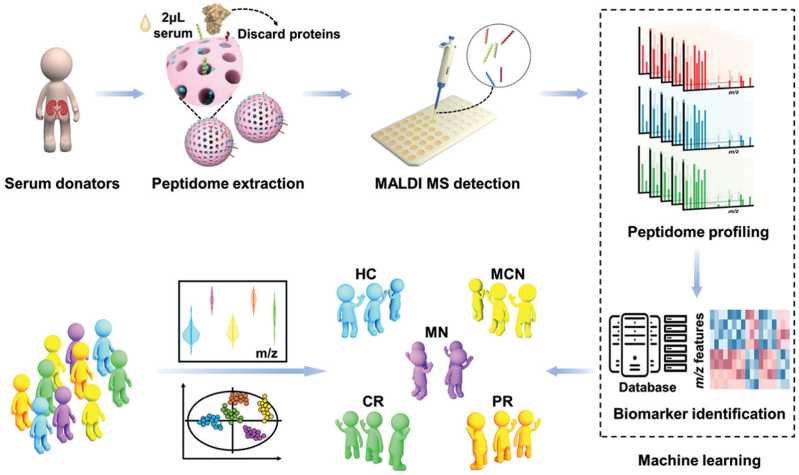

Fig. 1. The schematic illustration of MN monitoring *via* functionalized pore architecture-based peptidome profiling.

cision medicine is fast detection of large-scale clinical samples. In this regard, matrix-assisted laser desorption/ionization time-of-flight mass spectrometry (MALDI-TOF MS) is catching the eyes because of its rapid and high-throughput detection ability [23]. Recently, MALDI-TOF MS have been tentatively applied to exploratory construction of omics molecule-based diagnostic tool, and comparatively satisfactory results have been acquired, such as successful discrimination of disease samples from healthy controls (HC), or disease classification [24–27]. However, none of them has realized the comprehensive monitoring of diseases at the same time, which might be blamed for insufficient detection sensitivity deriving from the low abundance of targeted molecules and complexity of practical samples. To this end, nanomaterials with flexible design are continuously proposed and exploited, which is regarded as a good way to enrich targeted molecules and simplify samples. Peptidome, as the low-molecular proteome, is widely distributed throughout serum and associated with the real status of the entire organism [28]. For the moment, many researches have revealed that peptides were correlated with the emergence and development of diseases, and thereby being proposed to be prospective disease markers [29–31]. For instance, peptides of serum amyloid A-2, serum amyloid A-1, and C-reactive protein were reported to be capable of monitoring the severity of COVID-19 [32]. Fibrinogen α chain (605–629, *m/z* 2660), inter-α trypsin inhibitor heavy chain H4 (347–356, *m/z* 1061), apolipoprotein A-II (43–52, *m/z* 1041) were reported as serum peptides biomarkers for breast cancer [33]. As a result, we planned to realize the comprehensive individualized monitoring of MN using peptidome.

According to our previous research accumulation, Cu(II) ions can realize the all-round enrichment of peptides due to their outstanding coordination ability with carboxylic groups and amino groups of peptides [34]. Polydopamine (PDA) with numerous catechol functional groups can be formed and adhere to nearly any surface under mild conditions [35]. Moreover, PDA can be adjusted to highly open pore architecture by a soft templating method [36], with ability to make full use of itself functional groups for ion chelation [37]. Accordingly, an integrated approach of combining Cu(II) ions and porous polydopamine on magnetic core was proposed (denoted as Cu(II)-FPA) in this work. By taking advantage of numerous Cu(II) ions on the highly open pore architecture, fast magnetic responsiveness of magnetic core and MALDI-TOF MS, we successfully acquire peptidome data of hundreds of human serum, with rapidness and high efficiency. Combining with multiple machine learning algorithms, the comprehensive individualized monitoring of MN based on the global peptidome data can be realized with 100% sensitivity. Moreover, a defined peptide panel containing 12 specific feature signals has been constructed, achieving conventionally screening diagnosis, congeneric distinction and prognostic evaluation for MN. Excitingly, the sensitivity of the peptide panel in any group comparison is more than 97% that is comparable to global peptidome. And the unsupervised machine learning algorithm confirms the effectiveness of peptide panel, which is better than the global peptidome. This work provides a powerful means for comprehensive individualized monitoring of MN based on minimally invasive molecular detection, which will facilitate the development of molecular detection medicine.

The extraction of serum peptidome was implemented as seen in Fig. 1, during which the functionalized pore architecture plays the role of main contributor. The synthesis procedure of the functionalized pore architecture is displayed in Fig. S1a (Supporting information). Thereinto, the construction for the pore architecture made of polydopamine on magnetic core was the big highlight. Apart from the ability to directly conduct further functional immobilization with great convenience and enhance anti-interference performance, the specific pore architecture can provide large specific surface area to expand the loading capacity towards functional ions to enhance capture efficiency for peptidome. The field emission scanning electron microscope (FESEM) images in Figs. S1b and c (Supporting information) show evenly distributed porous structure, and the transmission electron microscope (TEM) images in Figs. S1d, and e (Supporting information) show uniform cylindrical-like mesopores are well-ordered and perpendicular to the surface of magnetic core. Such morphology characterizations illustrate the successful construction of the pore structure, which results in more exposed exterior surface. Furthermore, the Nitrogen adsorption-desorption isotherms in Fig. S1f (Supporting information) reveal the characteristic type IV curves, and the corresponding Brunauer–Emmett–Teller (BET) surface area is estimated to be 208.17 m^2/g. Such large specific surface area is enough to carry abundant functional copper ions for great peptidome capture. The element mapping images in Fig. S1g (Supporting information) well demonstrate the uniform distribution of Fe, C, N, O, and Cu elements in the pore architecture, indicating the practicability of the functionalized pore architecture in complete peptidome extraction [34].

In order to realize the comprehensive individualized monitoring of MN, we applied functionalized pore architecture to large-scale treatment of serum samples according to the schematic illustration of peptidome extraction. A total of 406 samples, including HC ($n = 171$), MN ($n = 124$) and other diseases closely related to MN ($n = 111$), were collected for serum peptidome extraction. In de-

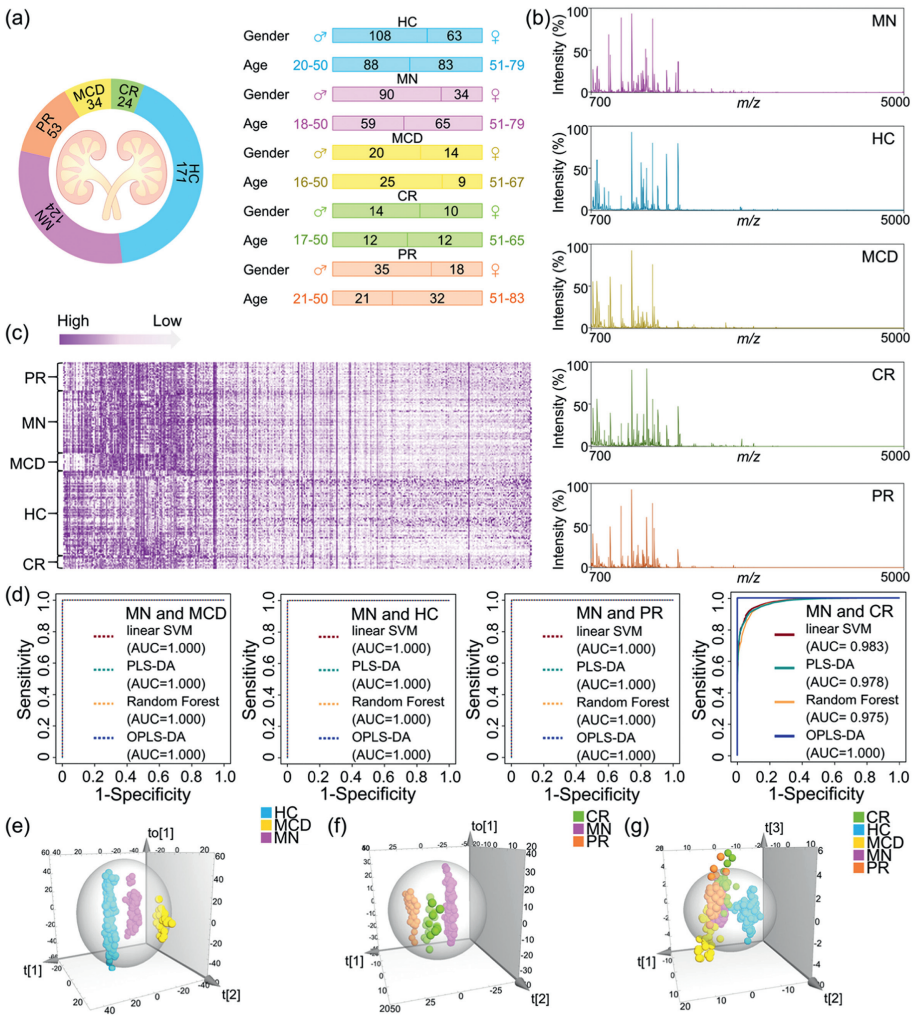

Fig. 2. Exploratory individualized monitoring of MN based on all *m/z* signals. (a) Brief clinical information of 406 samples. (b) Representative MS spectra of MN, HC, MCD, CR and PR. (c) Heatmap of all *m/z* signals in all the samples. (d) ROC curves of the discrimination in all samples between MN and MCD, MN and HC, MN and PR, MN and CR by different models including the linear SVM, PLS-DA, Random forests and OPLS-DA. 3D scatter plots in discovery cohort between (e) MN, MCD and HC; (f) MN, PR and CR; (g) MN, MCD, HC, PR and CR.

tail, other diseases refer to minimal change diseases (MCD, $n = 34$), partial remission of MN (PR, $n = 53$) and complete remission of MN (CR, $n = 24$). Thereinto, MN and MCD are two subtypes of primary nephrotic syndrome (PNS, $n = 158$), both of which possess similar clinical manifestation [38], and thereby being selected for comparison discrimination. PR and CR are uniformly defined as PC ($n = 77$), which are chosen for MN prognosis monitoring because they represent different degrees of remission after MN treatment. The brief information of all samples is displayed in Fig. 2a. According to Mann–Whitney *U* test, there is no significant difference for gender and age between MN and the other groups ($P > 0.05$, Tables S1–S4 in Supporting information). Additionally, in our study, PR and CR were treated with non-immunosuppressive therapy or immunosuppressive drugs, and there is no statistically significant distinction in the utilization of immunosuppressive drugs (Table S5 in Supporting information).

The typical MS spectra of HC, MN, MCD, PR, CR are displayed in Fig. 2b, in which the *m/z* region ranges from 700 Da to 5000 Da. After data pretreatment using RStudio, a total of 2800 *m/z* signals were defined, the global feature distribution is presented in Fig. 2c, showing the difference among different groups preliminarily.

An elementary exploration was firstly implemented to evaluate the screening possibility of MN from other four sample groups by applying four classical machine learning algorithms to all *m/z* signals, including linear support vector machines (SVM), partial least squares discriminant analysis (PLS-DA), random forests, and orthogonal partial least squares discriminant analysis (OPLS-DA). Surprisingly, all classifiers perform well. The corresponding receiver operating characteristic (ROC) curves of different machine learning models for MN discrimination were plotted. As shown in Fig. 2d, all models get quite high AUC values up to 1 when discriminating MN from MCD, HC, PR, and only OPLS-DA gets 1 for discrimination of MN from CR, other three models present slight decline fluctuation (0.983 for linear SVM, 0.978 for PLS-DA, 0.975 for random forest). These results indicated high screening feasibility of *m/z* signals extracted by Cu(II)-FPA for MN and OPLS-DA model was finally decided as the classifier for further exploration.

Then we divided all samples randomly into discovery cohort ($n = 131/98/27/42/19$, HC/MN/MCD/PR/CR) and validation cohort ($n = 40/26/7/11/5$, HC/MN/MCD/PR/CR), with aim to avoid overestimating performance of OPLS-DA model. As expected, clear separation of MN and other sample groups (HC, MCD, PC) in discovery cohort can be observed in OPLS-DA score plots (Fig. S2 in Supporting information). In addition to all corresponding $R^2Y(\text{cum}) > 0.92$, $Q^2(\text{cum}) > 0.87$, AUC = 1, the respective permutations with 200 iterations display that all right points are higher than those on

the left and the slopes of the regression line of Q^2 values are below zero, indicating that the OPLS-DA model is not overfitted. To further test the reliability of the OPLS-DA model, the respective validation cohorts are employed. As displayed in Fig. S3 (Supporting information), obvious clusters are visualized with reasonable model fitting, the corresponding R^2Y(cum) values are over 0.98, Q^2(cum) values over 0.77, and AUC values also reach 1. Furthermore, we explored the comprehensive monitoring possibility for MN by increasing sample group in discovery cohort. As shown in Fig. 2e, three-dimensional (3D) scatter plots show MN, HC and MCD are clustered separately (R^2Y(cum) = 0.97, Q^2(cum) = 0.929), plus the corresponding permutations in Fig. S4a (Supporting information), indicating high diagnostic value of serum peptide features. Besides, the 3D scatter plots among MN, PR, and CR (R^2Y(cum) = 0.953, Q^2(cum) = 0.69, Fig. 2f) and the corresponding permutations (Fig. S4b in Supporting information) suggest the prognosis monitoring value of serum peptide features. Finally, we made an exploration on the discrimination of all sample groups. As seen in Fig. 2g and Fig. S4c (Supporting information), the 3D scatter plots among MN, MCD, HC, PR and CR (R^2Y(cum) = 0.686, Q^2(cum) = 0.605) and the corresponding permutations suggest the comprehensive monitoring potential of serum peptide features for MN. Similarly, to further test the reliability of the above results, the individual validation cohorts are applied respectively. In detail, the 3D scatter plots among MN, HC and MCD (R^2Y(cum) = 0.976, Q^2(cum) = 0.865) and the corresponding permutations are displayed in Figs. S5a and b (Supporting information), the 3D scatter plots among MN, PR, and CR (R^2Y(cum) = 0.983, Q^2(cum) = 0.718) and the corresponding permutations are displayed in Figs. S5c and d (Supporting information), the 3D scatter plots among MN, MCD, HC, PR and CR (R^2Y(cum) = 0.956, Q^2(cum) = 0.701) and the corresponding permutations are displayed in Figs. S5e and f (Supporting information).

Inspired by the results of all *m/z* signals in MN comprehensive monitoring, we attempted to screen out important features with high specificity and sensitivity for further clinical application exploration. All *m/z* signals of discovery cohort through designed pairwise comparison among sample groups are firstly subjected to various feature selection algorithms to be sorted, including *t*-test of the expression level analysis, fold change (FC) analysis, variable importance on projection (VIP) analysis. Thereinto, the volcano plots of the differential expression between HC and PNS, MN and MCD, HC and PC, MN and PC, CR and PR in discovery cohort were depicted, which show the conspicuous up- and down- regulation of all *m/z* signals (Fig. S6 in Supporting information). Afterwards, the intersection of five pairwise comparison combining VIP > 1, FC > 2 or FC < 0.5 and $P < 0.05$ was selected to construct feature signal panel, the criterion for selecting biomarkers is shown in Fig. S7a (Supporting information). As a result, 12 specific feature signals are finally selected to act as the panel, the heatmap of which in all samples shows they may make a great contribution to comprehensive monitoring of MN, including conventional diagnosis, congeneric distinction and prognosis evaluation (Fig. S7b in Supporting information). Moreover, the distribution violin plots of these 12 specific feature signals are depicted. As Fig. S7c (Supporting information) displayed, each feature contributes variance to MN comprehensive monitoring.

In order to confirm the construction validity of the panel briefly, MN are respectively differentiated from HC, MCD, PC in discovery cohort with sensitivity of 98%, 100%, 97% and specificity of 97%, 100%, 97% respectively. Fig. S8 (Supporting information) shows that the OPLS-DA score plots between MN and HC (R^2Y(cum) = 0.791, Q^2(cum) = 0.782, AUC = 0.998), MN and MCD (R^2Y(cum) = 0.917, Q^2(cum) = 0.91, AUC = 1) and MN and PC (R^2Y(cum) = 0.806, Q^2(cum) = 0.786, AUC = 0.987). Then we tested the performance of the panel in MN detection by using the validation cohort. As seen in Fig. S9 (Supporting information), the relatively satisfactory cluster separation and AUC values are attained, with outstanding interpretability and predictability. In detail, the discrimination of MN and HC achieves AUC of 0.999 (R^2Y(cum) = 0.811, Q^2(cum) = 0.767, 98% of sensitivity, 100% of specificity), the discrimination of MN and MCD achieves AUC of 1(R^2Y(cum) = 0.89, Q^2(cum) = 0.86, 100% of sensitivity, 100% of specificity), and the discrimination of MN and PC achieves AUC of 1 (R^2Y(cum) = 0.937, Q^2(cum) = 0.93, 100% of sensitivity, 100% of specificity). Next, we visualized the discrimination results of MN *versus* multiple sample groups in both discovery cohort and validation cohort. One exciting result is that, as shown in Figs. S10a–d (Supporting information), the 3D scatter plots exhibit that the conventional diagnosis and congeneric distinction of MN from HC and MCD can be realized simultaneously (discovery cohort: R^2Y(cum) = 0.798, Q^2(cum) = 0.789; validation cohort: R^2Y(cum) = 0.811, Q^2(cum) = 0.75), confirming the good credibility of the constructed panel. Moreover, Figs. S10e–h (Supporting information) show the prognosis monitoring towards MN also can be realized based on the panel (discovery cohort: R^2Y(cum) = 0.591, Q^2(cum) = 0.562; validation cohort: R^2Y(cum) = 0.817, Q^2(cum) = 0.672). As well, the comprehensive monitoring of MN which was distinguished from HC, MCD, PR, CR is basically achieved based on the panel (Figs. S10i–l in Supporting information), discovery cohort: R^2Y(cum) = 0.537, Q^2(cum) = 0.516, average AUC is 0.988 and average f1 score is 0.884; validation cohort: R^2Y(cum) = 0.629, Q^2(cum) = 0.578), average AUC is 0.993 and average f1 score is 0.932. Of note, the values of R^2Y(cum) and Q^2(cum) present decrease when concerning the prognosis data, which probably is caused by the limited sample number. Nevertheless, the above results still confirm the feasibility of comprehensive individualized monitoring of MN by functionalized pore architecture-based peptidome profiling.

Encouraged by the above results, we exerted principal component analysis (PCA), an unsupervised machine learning algorithm, between MN and other four sample groups. As comparison, the PCA based on both all *m/z* signals and 12 specific feature signals are applied. As seen in Figs. S11a–d (Supporting information), MN cannot be separated from MCD, HC, PR, and CR based on all *m/z* signals. However, the obviously improved separation situation between MN and any other sample group can be observed based on 12 specific feature signals (Figs. S11e–h in Supporting information). Basically, the two groups gather in the respective areas within 95% confidence interval.

In particular, the clear group separation can be directly perceived through the senses for MN *versus* MCD and MN *versus* PR. The first two principal components can explain 64.0% and 13.8% for MN and MCD, as well as 57.1% and 19.3% for MN and PR, which are greater than that from all *m/z* signals (14.4% and 11.6% for MN and MCD, 14.3% and 12.7% for MN and PR). Besides, the interpretability of the first two principal components also increased from 27.8% to 67.2% for MN versus HC, from 27.9% to 63.3% for MN versus CR, respectively. All these phenomena confirm the high responsibility of 12 specific feature signals towards difference revelation, namely their remarkable diagnosis and prognosis ability.

Afterwards, we conducted further exploration and validation for these specific feature signals. Preliminarily, we combined LC-MS/MS with Uniprot to identify these specific peptide features. The serum samples from two MN, two MCD, two HC, two PR and two CR were collected. After enrichment by Cu(II)-FPA, the eluent was lyophilized and desalted, followed by Nano-HPLC-MS/MS analysis and Uniprot-SwissProt database searching. The detailed annotation information of 12 biomarkers is listed in Table S6 (Supporting information), which shows that these specific peptide features are respectively identified as protein fragments of haptoglobin, fibrinogen alpha chain, apolipoprotein C3, albumin, apolipoprotein L1,

prothrombin, complement C3, transthyretin. Combined with previous reports, the matching results indicate the reasonability of these specific peptide features in MN moitoring. Notably, the well-known Complement C3 is considered as the key substance of the classical pathway and the alternative pathway [39], the expression level of which has been clearly reported to be a sign for distinguishing MN and MCD [40]. Apolipoprotein L1 is produced primarily in the liver and circulates in the high-density lipoprotein (HDL) [41]. According to reports, the direct reflection of dysregulation Apolipoprotein L1 is the elevation of HDL endocytic receptor or deficiency of HDL docking receptor, which are caused by MN, MCD or other glomerular filtration barrier diseases [42]. Haptoglobin, which is involved in the physiological defense against hemoglobin-induced renal toxicity, has been discussed as a new therapeutic target for MN [43]. Additionally, apolipoprotein C3 and prothrombin were reported to be associated with patient situation of MN. The former affects MN development by promoting the secretion of low density lipoproteins and increasing the expression of cholesterol accumulation [44]. The latter progresses MN by regulating the expression of macrophage migration inhibitory factor that exerts a key regulatory function in the pathogenesis of MN [45]. Transthyretin was reported to be the candidate biomarker of nephrotic syndrome [46], and mutant fibrinogen alpha chain was regarded to be a coordinator of proteinuria which is a singnificant indicator of MN, morever, mutant fibrinogen alpha chain is related to renal failure [47]. Besides, the level of serum albumin is considered as an early predictor for prognostic evaluation of MN [48].

In conclusion, we proposed a peptidome analysis means for realizing comprehensive individualized monitoring of MN. In this work, Cu(II)-FPA, which possessed highly open porous channels and numerous Cu(II) ions, was constructed and applied to capture peptides from a large number of human serum samples. Further combined with MALDI MS and machine learning algorithms, peptidome differences in different groups were inspected. With all peptidome features, the OPLS-DA machine learning model could discriminate MN from HC, MCD, PR and CR, respectively, with AUC values up to 1 for both the discovery cohorts and validation cohorts, confirming excellent accuracy and practical prediction ability. Moreover, when applying the important measure (VIP >1, FC >2 or FC <0.5 and $P<0.05$) in OPLS-DA model, 12 specific peptide features significantly contributing to model classification were screened out from the intersection of features of HC and PNS, MN and MCD, MN and PC, HC and PC, PR and CR. MN detection and prognosis evaluation was realized based on the 12 specific peptide features in OPLS-DA model with the sensitivity and specificity ranging from 97% to 100%. Additionally, PCA analysis exhibits obviously improved separation situation. Heatmap and violin plots further manifest the differential expression of identified biomarkers in MN, MCD, HC, PR and CR. The LC-MS analysis of these 12 specific peptide features proves their close association with MN. All the above verifies the reliability and practicability of the key peptide features. This work provides guidance for clinical means exploration and inspires peptidome analysis protocols towards precise diagnosis and prognosis of diseases.

Ethical statement

This study strictly adhered to the principles of Helsinki Declaration and was approved by the Ethics Committee of Huashan Hospital, Fudan University (2016-394-1). In addition, all volunteers and patients who participated in this work agreed to provide serum samples for the study.

Declaration of competing interest

The authors declare that they have no known competing financial interests or personal relationships that could have appeared to influence the work reported in this paper.

Acknowledgments

This work was financially supported by National Key R&D Program of China (No. 2018YFA0507501) and the National Natural Science Foundation of China (Nos. 22074019, 21425518, 22004017), and Shanghai Sailing Program (No. 20YF1405300).

Supplementary materials

Supplementary material associated with this article can be found, in the online version, at doi:10.1016/j.cclet.2023.108975.

References

[1] E. Hoxha, L. Reinhard, R.A.K. Stahl, Nat. Rev. Nephrol. 18 (2022) 466–478.
[2] A. Schieppati, L. Mosconi, A. Perna, et al., New Engl. J. Med. 329 (1993) 85–89.
[3] L.H. Beck, R.G.B. Bonegio, G. Lambeau, et al., New Engl. J. Med. 361 (2009) 11–21.
[4] S. Sethi, J. Am. Soc. Nephrol. 32 (2021) 268–278.
[5] A.S. De Vriese, R.J. Glassock, K.A. Nath, et al., J. Am. Soc. Nephrol. 28 (2017) 421.
[6] R.J. Glassock, Semin. Nephrol. 23 (2003) 324–332.
[7] P.D. Burbelo, M. Joshi, A. Chaturvedi, et al., J. Am. Soc. Nephrol. 31 (2020) 208.
[8] P. Ronco, L. Beck, H. Debiec, et al., Nat. Rev. Dis. Primers 7 (2021) 69.
[9] E. Hoxha, L.H. Beck, T. Wiech, et al., J. Am. Soc. Nephrol. 28 (2017) 520.
[10] C. Li, Z. Yao, M. Zhu, et al., Kidney Blood Press. Res. 42 (2017) 1045–1052.
[11] B. Basu, A. Angeletti, B. Islam, et al., Front. Immunol. 13 (2022) 805697.
[12] J.B. Kopp, H.-J. Anders, K. Susztak, et al., Nat. Rev. Dis. Primers 6 (2020) 68.
[13] L. Kuo Ramsay, E. Lingeman James, P. Evan Andrew, et al., J. Urol. 170 (2003) 2186–2189.
[14] F. Scolari, E. Delbarba, D. Santoro, et al., J. Am. Soc. Nephrol. 32 (2021) 972–982.
[15] F.C. Fervenza, G.B. Appel, S.J. Barbour, et al., N. Engl. J. Med. 381 (2019) 36–46.
[16] D.C. Cattran, J. Feehally, H.T. Cook, et al., Kidney Int. Suppl. 2 (2012) 139–274.
[17] M.M. Rinschen, J. Ivanisevic, M. Giera, G. Siuzdak, Nat. Rev. Mol. Cell Biol. 20 (2019) 353–367.
[18] A.J. Vargas, C.C. Harris, Nat. Rev. Cancer 16 (2016) 525–537.
[19] C.J. Houldcroft, M.A. Beale, J. Breuer, Nat. Rev. Microbiol. 15 (2017) 183–192.
[20] W. Stephenson, L.T. Donlin, A. Butler, et al., Nat. Commun. 9 (2018) 791.
[21] X. Hu, Z. Wang, H. Chen, et al., Anal. Chem. 94 (2022) 14846–14853.
[22] J. Cao, X. Shi, D.D. Gurav, et al., Adv. Mater. 32 (2020) e2000906.
[23] H. Chen, C. Huang, Y. Wu, et al., ACS Nano 16 (2022) 12952–12963.
[24] L. Niu, M. Thiele, P.E. Geyer, et al., Nat. Med. 28 (2022) 1277–1287.
[25] D.L. Church, L. Cerutti, A. Gürtler, et al., Clin. Microbiol. Rev. 33 (2020) e00053-19.
[26] Z. Xu, H. Chen, H. Chu, et al., Chin. Chem. Lett. 34 (2023) 107829.
[27] L. He, X. Wang, J. Chen, et al., Anal. Chem. 94 (2022) 10367–10374.
[28] Y. Li, N. Sun, X. Hu, et al., Trends Anal. Chem. 120 (2019) 115658.
[29] Y. Xu, J. Yan, Y. Tao, et al., Science 377 (2022) 1085–1091.
[30] Z. Wang, C. Huang, N. Sun, C. Deng, Sci. China Chem. 64 (2021) 932–947.
[31] R. Liu, P. Wei, C. Keller, et al., Anal. Chem. 92 (2020) 14021–14030.
[32] B. Shen, X. Yi, Y. Sun, et al., Cell 182 (2020) 59–72.
[33] J. Yang, X. Xiong, S. Liu, et al., Proteomics 16 (2016) 925–934.
[34] S. Liu, H. Chen, X. Lu, et al., Angew. Chem. Int. Ed. 49 (2010) 7557–7561.
[35] N. Sun, H. Wu, X. Shen, C. Deng, Adv. Funct. Mater. 29 (2019) 1900253.
[36] P. Pan, T. Zhang, Q. Yue, et al., Adv. Sci. 7 (2020) 2000443.
[37] P. Qiu, B. Ma, C.T. Hung, et al., Acc. Chem. Res. 52 (2019) 2928–2938.
[38] F. Chen, D. Wu, R. Wang, et al., Blood 134 (2019) 5696.
[39] Y.-S. Kang, Y. Do, H.-K. Lee, et al., Cell 125 (2006) 47–58.
[40] F. Wu, Y. Zhang, W. Cu, et al., Sci. Rep. 11 (2021) 18064.
[41] I.S. Daehn, J.S. Duffield, Nat. Rev. Drug Discov. 20 (2021) 770–788.
[42] F. Wu, Y. Zhang, W. Cui, et al., Sci. Rep. 11 (2021) 18064.
[43] H.H.-Y. Ngai, W.-H. Sit, P.-P. Jiang, et al., J. Proteome Res. 6 (2007) 3313–3320.
[44] D. Wu, Z. Yu, S. Zhao, et al., Clin. Sci. 133 (2019) 1255–1269.
[45] N. Ding, P.L. Li, K.L. Wu, et al., Sci. Rep. 12 (2022) 1558.
[46] S.A. Varghese, T.B. Powell, M.N. Budisavljevic, et al., J. Am. Soc. Nephrol. 18 (2007) 913–922.
[47] M.M. Picken, R.P. Linke, J. Am. Soc. Nephrol. 20 (2009) 1681–1685.
[48] G. Stefan, S. Stancu, A. Zugravu, et al., Ren. Fail. 44 (2022) 258–268.